FULL LENGTH PAPER

PREDICTION OF HELICOPTER BLADE LOADS FOR AN UNSTEADY PULL-UP MANEUVER USING LIFTING-LINE AND CFD/CSD ANALYSES

Abhishek
Assistant Professor
Department of Aerospace Engineering
Indian Institute of Technology Kanpur
Kanpur-208 016, India
Email : abhish@iitk.ac.in

Abstract

This paper investigates the aeromechanics of a prescribed 2.1g pull-up maneuver for a helicopter rotor. The simulation is carried out using multibody based Computational Structural Dynamics (CSD) model tightly coupled to a high-fidelity Computational Fluid Dynamics (CFD) solver. The predictions are also compared with those obtained using lifting-line based comprehensive analysis to highlight the capabilities of a high-fidelity simulation. The results show considerable improvements in the predicted results by using a CFD model over a traditional lifting-line approach. In particular, coupled CFD/CSD simulation is able to correctly predict the magnitude and phasing of the two dynamic stall cycles on the retreating side of the rotor disk during the maneuver. Further, it shows significant improvement in the predicted peak-to-peak structural loads. The advancing blade stall is not predicted by either of the analysis. The study also shows some deficiencies in the ability to predict blade torsional loads.

Nomenclature

C_T = Thrust coefficient
μ = Advance ratio
σ = Rotor solidity
θ_0 = Collective pitch angle
θ_{lc} = Lateral cyclic pitch angle
θ_{ls} = Longitudinal cyclic pitch angle

Introduction

The main rotor structural loads encountered during unsteady maneuvers are important to size different critical components of the rotor system, particularly for advanced combat helicopters. These include the blade structural loads, control/pitch-link loads, and swashplate servo loads. Accurate and consistent prediction of maneuver loads is necessary to reduce the risks and costs associated with use of prior flight test data as a basis for design.

The state -of-the-art prediction of main rotor loads in steady level flight - critical for vibratory loads - using Computational Fluid Dynamics (CFD) / Structural Dynamics (CSD) coupled analysis can be found in [1]. Loads prediction in unsteady maneuvers - critical for peak design loads - has remained a challenging task. Accurate analysis and prediction of loads mechanisms in an unsteady maneuver is a major barrier in the field of rotor aeromechanics, primarily due to the following two reasons: 1) several complex aerodynamic phenomena can occur simultaneously in a maneuver, and 2) an inverse solution procedure to determine the trim variables (pitch control angles, vehicle attitude angles, and yaw control) in order to fly a prescribed trajectory is quite involved and not yet available to a satisfactory level. In a steady level flight, the trajectory is simple, and the aircraft Euler equations reduce to six equilibrium equations from which the trim variables are determined successfully, such is not the case in a maneuvering flight. The complexity of the solution procedure has been the primary hurdle for a first principles prediction of maneuver loads. Today, extensive flight test data such as the U.S. Army/NASA Airloads Program [2,3] has opened opportunity to bypass this complexity. The measured values of rotor controls, aircraft attitudes, and

Paper Code : V65 N2/784-2013. Manuscript received on 20 Jun 2012. Reviewed, revised and accepted as a Full Length Contributed Paper on 10 Dec 2012

flight trajectory can now all be prescribed from flight test data in order to focus solely on the loads mechanisms.

The maneuvers with highest loads of the UH-60A Black Hawk helicopter have been studied in great detail by Bousman et al. [4,5]. Based on the criteria of six structural measurements: pitch-link load, torsion moment (30% R), and flap and chord bending moments (11.3% R and 60% R), they identified and ranked the severest maneuvers. Out of the two severest maneuvers, the second most severe maneuver, designated by Counter 11029, which is based on the Utility Tactical Transport Aerial System (UTTAS) maneuver of the original UH-60A design specification, is studied in this paper. It is a dynamic pull-up that reaches 2.12g at 139 knots and produces the highest root flap bending moment and the third highest oscillatory pitch-link load of all the UH-60A maneuvers. The measured load factor and velocity ratio are shown in Figs.1 and 2. Even though the pitch-link load is only third highest of all the maneuvers, it still exceeds the loads encountered in operational use. For example, the peak-to-peak pitch link loads at this flight are 20% higher than those encountered during free engagement air-to-air combat test (AACT) flights of similar kind [6]. The aircraft attitude angles and angular rates are shown in Figs.3(a) and 3(b). The aircraft pitch angle when reduced using the measured flight path angle (not shown) and a 3° forward built-in shaft angle produces the effective shaft tilt with respect to the on-coming flow, Fig.4. The wake is expected to pass through the rotor disk around revolutions 10 and 24 - first from below to above and then from above to below.

A high fidelity simulation of the prescribed UTTAS pull-up was carried out by Bhagwat et al. [7,8], using a multibody finite element structural model coupled with a Reynolds Averaged Navier-Stokes (RANS) model. This work demonstrated RANS capability in predicting two rotor dynamic stall cycles for the first time for a maneuver, and showed that the oscillatory blade structural loads could be predicted with increased accuracy using an isolated rotor calculation. Ref.[9] carried out a simpler lifting-line analysis, also for an isolated rotor, with an attempt to calculate the rotor pitch control angles. However, it was unsuccessful, due to large errors stemming from the unknown horizontal tail lift during the maneuver, and an inability to predict the maneuver trajectories in absence of detailed aircraft data. Subsequently, with availability of flight test control angles, several researchers have predicted loads for this prescribed maneuver - [10,11] focused on lower fidelity lifting-line predictions, [12,13] employed wake-coupling CFD/CSD approach and Silbaugh [14] examined the effect of time-accurate coupling using RANS.

The objective of the present work is to systematically analyze the aeromechanics of a prescribed maneuver for UH-60A helicopter. The unsteady evolution of the blade aerodynamic and structural response to time-varying pilot inputs was consistently coupled to obtain the aeroelastic solution to the maneuver. A multibody based finite element structural model, is used to predict the blade structural motion. The predictions from conventional lifting line methodology is compared with those obtained from a high-fidelity CFD solver (OVERTURNS) to gain a better insight into the limitations of the conventional aerodynamic solvers.

Methodology

The complexity of the aeroelastic rotor problem renders a full continuum dynamics solution impractical. Therefore, a domain partitioning approach is used to simplify the solution process by using domain-specific solvers that solve the fluid and structural governing equations separately using the most efficient solution strategy for the specific domain. The partitioned domains interact at the fluid-structure interface to provide the fully-coupled aeroelastic response of the rotor.

Rotor Structural Dynamics Model

The rotor structural dynamics model uses a full finite element analysis based on multi - body formulation [15,16]. The second order non-linear beam model used is same as the one used in [22]. The rotor model (Fig.5) consists of flexible blades, rigid root end control components, and a swashplate model. Each blade is modeled as a fully articulated beam with coincident flap and lag hinges. It is discretized using 20 nonlinear beam elements, and each nonlinear beam elements has a local frame of reference attached to it, to model arbitrary large deformations. The blade dynamics equations are updated to include the gyroscopic contributions to the rotor resulting from the vehicle linear and angular accelerations. The swept portion of the blade is modeled using 3 elements with swept elastic axis. The pitch horn and the hub are modeled using rigid bodies and the pitch-link is modeled as a linear spring-damper element. The pitch-link stiffness is obtained using the measured equivalent root torsion spring stiffness of 1090 ft-lbs/deg [23]. The blade property

data were obtained from the NASA (Ames) master database.

Lifting-line Aerodynamic Model

The lifting line aerodynamic model used in this study involves a Weissinger, L [24] type lifting-surface model iteratively coupled to 2D airfoil tables (scaled near wake), Leishman-Beddoes 2D unsteady aerodynamics for attached and separated flows [25], and a time accurate free wake model [26] based on Ananthan and Leishman [27]. A single tip vortex trailer is used for the present analysis. The lifting-surface model is refined to include the effects of vehicle roll and pitch rates.

At each azimuth (i.e. time), the inputs into the lifting-line analysis are the blade deformations for all blades, the instantaneous advance ratio, shaft tilt angles, the rotor pitch and roll angles and angular rates, and the control angles. The outputs from the model are the airloads occurring on all blades, and the inflow velocities at the blade control points (3/4 chord line) on all blades, at that instant. Within the model, the airloads are calculated using the inflow velocities obtained in the previous time step. The current blade deformations are used along with inflow velocities stored from the previous time step to calculate the airloads, bound circulation distribution, near wake trailer strengths, and near wake induced velocities at the blade control points. The near wake induced velocities are then used to re-calculate the airloads. The bound circulation distribution and the current blade deformations are then used to advance the free wake solution to the present time step. This free wake solution is then used in the calculation of airloads in the next time step. The airloads at the present time step are re-calculated including the near wake induced velocities. The effect of shed wake is incorporated using an unsteady aerodynamic model. At each time step, the unsteady model is updated based on the change in airloads from the previous time step. The Leishman-Beddoes unsteady model (for attached and separated flows) is used in the present analysis. The numerical solution procedure of the free wake is same as that of the Ananthan-Leishman model, validated [27]. However, the present formulation incorporates flexible blade deformations in flap, lag, and torsion, and the vortex strengths and boundary conditions are prescribed.

Reynolds-Averaged Navier-Stokes CFD Solver

The baseline CFD solver used for the present work is the overset, structured mesh, unsteady RANS solver OVERTURNS (OVERset Transonic Unsteady Rotor Navier-Stokes). Time integration is performed using a second-order backward difference method using Lower-Upper Symmetric Gauss Seidel (LUSGS) [28]. Eight Newton sub-iterations are used to remove factorization errors and recover time accuracy for unsteady computations [29]. The inviscid fluxes are computed using an upwind scheme that uses Roe's flux differencing with MUSCL type limiting. The viscous fluxes are computed using second-order central differencing. The Baldwin-Lomax turbulence model is utilized for RANS closure. The effects of maneuver are incorporated using source terms in the Navier-Stokes equation using non- inertial frame of reference [14]. The blade motions are accounted for by mesh rotation to account for blade rotational speed and mesh deformations are applied via exact surface mapping on the blade, which decays away from the blade surface to the outer boundary of the blade meshes.

The solver uses an overset mesh system for efficient wake capturing. In this arrangement, the body-fitted blade meshes are embedded inside a cylindrical off-body mesh to capture the entire rotor blade-wake aerodynamics (Fig.6). The body conforming C-O meshes ensures a better definition of the blade tips, and consists of 129 points in the wraparound direction (of which 97 points are on the blade surface), 129 points in the spanwise direction, and 65 points in the normal direction. The spacing of grids near the blade surface in the normal direction is approximately 10^{-5} chord which is required for the viscous calculations. The background mesh is composed of four overlapping cylindrical quadrants with 49x99x110 in the azimuthal, spanwise, and normal direction respectively, this amounts to a total of 4.8 million grid points, including the blade mesh points.

The coupling between the different solvers (structural and CFD) is achieved using Python scripts. Each solver provides a Python class interface which interacts with the FORTRAN modules using FORTRAN to Python Interface generator (F2PY). Parallelized execution of the code is achieved using pyMPI. The Python NumPy library is used for general array manipulation and data exchange between the solvers. The interpolation of the deformation for grid motion at each time step is done using the structural solver for the specified grid locations. This ensures the consistency between grid deformation and beam deformation kinematics. To minimize grid movement near the outer boundary of the body fitted grids, a decaying radial function is applied to the beam kinematic parameters.

Solution Procedure

The solution procedure for the coupled analysis of maneuver starts with a periodic solution for the first revolution which corresponds to steady flight condition. The steady periodic solution is obtained by marching in time with the calculated trim angles for rev.1 of the maneuver, by letting the analysis run for 6 revolutions. At least 5 - 6 revolutions are needed for the lightly damped lag-mode to stabilize. Once the dynamic response settles into periodicity, then, the maneuver is initiated by smoothly merging the control angles from the level flight condition. The velocity ratio, shaft angles, attitudes, and rates are subsequently prescribed using the test conditions. During the maneuver, the structural dynamic and the aerodynamic models are advanced in time after exchanging deformations and airloads at every time step. No sub-iterations are employed to ensure strict time accuracy, i.e. deflections at a given azimuth are calculated based on airloads from the previous azimuth. The calculated deflections are then used to advance the airloads to the current azimuth. The deflections, however, are not updated based on current azimuth airloads. Note that this procedure is also referred to as loose coupling by the fixed wing CFD/CSD researchers [30].

The level flight at the beginning of the maneuver is simulated using calculated rotor control angles using conventional trim analysis. The trim angles thus obtained are then used to adjust the control angles obtained from the flight test. In this approach the entire control time history for the maneuver is corrected to match the initial trim angles. The time history of control angles used for CSD/lifting-line analysis are shown in Fig.7.

Results

The UTTAS pull-up maneuver is initiated from a steady, level flight condition with an advance ratio μ = 0.357, and a blade loading coefficient $C_T/\sigma = 0.0793$. The solution is obtained by marching in time and the instantaneous values of blade control pitch settings, transient velocities, vehicle attitude and attitude rates are prescribed as inputs to the structural and aerodynamic solvers. Note that rather than specifying the actual control pitch settings obtained from the flight test data, shown in Table-1, the time histories are corrected using a constant offset such that the values correspond to the trim solution predicted by the CFD/CSD analysis at time t = 0. Both lifting line analysis and CFD solver are coupled with CSD to analyze the differences in the aerodynamic models.

Table-1 : Trim Solutions Predicted by Different Simulations for the Initial Steady Phase of the UTTAS Pull-up Maneuver

	Collective θ_0	Longitudinal Cyclic θ_{ls}	Lateral Cyclic θ_{lc}
Flight Test	12.32	-9.78	4.68
CSD/Lifting-line	14.29	-8.76	3.06
CFD/CSD	15.41	-9.13	4.29

Blade Airloads

The study of C11029 maneuver can be divided into three different phases. The initial 5 revolutions are steady, with the pitch and roll angles remaining nearly constant, and would be referred as the steady flight regime. The unsteady phase starts around revolution 6, with helicopter attaining high pitch rate and linear acceleration with tip-path-plane tilting backwards. The vehicle load factor crosses 2.0g towards the beginning of revolution 13, and remains above 2.0g till revolution 18 and would be called the maneuvering flight regime. After which the vehicle tries to attain back its original steady level flight attitude, which constitutes the third and final phase.

Steady Flight Regime

This section compares the airloads predicted during the steady phase of the maneuver. The airloads at all the eight flight test radial-stations are compared. Figs.8, and 9 show the time histories of the normal force and pitching moment predicted by two different simulations: 1) coupled CSD with lifting-line analysis (shown in red), and 2) coupled CFD/CSD analysis (shown in blue). The analysis with lifting line aerodynamics was performed at a time-step of 2.0o, while the CFD/CSD analysis was performed at a time-step of 0.25o. The lifting-line analysis is unable to resolve the phasing of the negative lift peak adequately. This is primarily due to the inaccurate elastic twist, which in turn is due to the inaccurate pitching moment prediction by the lifting-line analysis. It can be observed that the lifting-line analysis is unable to accurately predict the large positive to negative moment oscillation on the advancing side near the tip. This behavior is a result of the effect of 3D relief on unsteady formation and collapse of shocks on the advancing blade [14], a 3D phenomenon, which is not properly accounted for in the lifting-line

model. The inadequacy of the lifting-line model in this region is well documented in literature [34]. CFD/CSD coupled analysis on the other hand is able to accurately predict the 3D unsteady transonic pitching moment.

Maneuvering Flight Regime

Figures 10 and 11 show the time history of normal force at 86.5% radial station, predicted using the CFD/CSD coupled analysis and lifting-line analysis. The high-fidelity analysis is able to predict the higher harmonic stall loads, which are primarily 4, and 5/rev during the maneuvering flight regime, which are missed by the lifting-line model.

Figures 12 to 15 compare the predictions using CFD/CSD with those obtained using lifting-line analysis at 77.5%R and 86.5%R spanwise stations. The prediction using lifting-line analysis shows, in Figs.12 and 13, 'relatively' improved correlation with the flight test data at 77.5%R station than compared to the lifting-line prediction at 86.5%R which are shown in Figs.14 and 15. While, the lifting-line analysis is able to capture the trends of the waveform correctly, the stall magnitude is under-predicted all through the maneuver.

It is also observed that at 86.5%R station the CFD/CSD analysis is able to consistently predict the two retreating stall cycles, Fig.16(d). The pull-up maneuver is characterized by three stall cycles occurring across the rotor disk, with first stall cycle occurring on the advancing side, followed by two dynamic stall events on the retreating side, as shown by the darker regions in the flight test contour plot for the non-dimensional pitching moment for the revolution 14, (Fig.16(c)). The CFD/CSD analysis is showing fair correlation for the peak magnitude of the stall loads. The airloads time histories, particularly the pitching moments, clearly indicate the dynamic stall phenomenon as the dominant aerodynamic characteristic of the UTTAS maneuver. To gain further insight into the severity and the extent of this stall across the rotor disk, the variations of the pitching moments across the rotor disk at the peak of the maneuver, Fig.16(c), is compared with the conditions observed in the steady flight conditions, Fig.16(a). The pitching moment variations during steady flight conditions are benign and show no steep gradients across the rotor disk. During this phase, the CFD/CSD analysis shows good correlation with the flight test data, Fig.16(b). In contrast, the pitching moment contours for rev.14 of the flight test data show steep gradients in the first and fourth quadrants indicating moment stall near the blade tips. While the flight test data appears to indicate that the stall is restricted to the outermost regions of the retreating side, the CFD/CSD analyses predict a much more widespread region of moment variations. This could be because of the low spanwise resolution of the flight test data (only nine radial stations across span). The third stall event seen as a pronounced down-up gradient in the first quadrant is missed by both the computational analyses.

The predicted chord force at 86.5% radial station is shown in Fig.17. In general, the prediction shows good correlation with the flight test data, but the peak-to-peak magnitude is over-predicted, this could stem from the fact that the lag-dynamics of UH-60A rotor is significantly influenced by the non-linear lag damper, which is not included in the present structural model.

Attitude Recovery Phase - The Lift Deficiency Problem

It is important to note that a deficiency in the predicted mean normal forces during the attitude recovery phase of the maneuver has been reported by several researchers [11,12]. A similar discrepancy is also observed in the linearized aerodynamic analysis conducted using the coupled CSD/lifting-line analysis discussed earlier, but not in the coupled CFD/CSD analysis (Fig.18). The reason for this may be attributed to the fact that the lifting-line analysis always under-predicts the pitching moment stall magnitude by a significant margin, thereby introducing errors in the steady elastic twist response which accumulates over the period of time to cause a net deficiency in the angle of attack resulting in reduced mean lift towards the end of the maneuver.

Blade Structural Loads

Predictions of the structural bending moments during the steady phase are shown in Fig.19. The flap bending moment is almost entirely determined by the predicted lift. While, the predictions using the CFD/CSD simulation, shows good agreement with the flight test, the results from the lifting-line model show poor correlation, with a peak-to-peak under-prediction by 26%. In the absence of non-linear lag damper model, both the predictions for the lag bending moments are less satisfactory, as it is dominated by the lag damper force. The predicted torsion moment using CFD/CSD analysis is showing good correlation with the flight test, the predictions using the lifting-line analysis also shows peak-to-peak correlation with an under-predic-

tion of only 10%, however the waveform is less satisfactory on the retreating side.

As with the steady flight results, the predicted flap bending moment using the CFD/CSD analysis shows good correlation with the flight test (Figs.20 and 21). There is an over-prediction in the peak-to-peak magnitude of the lag bending moment after revolution 7 as shown in Figs.22 and 23. Further, the waveform shows poor correlation with the flight test towards the later part of the maneuver. The torsion moment time history is shown in Figs.24 and 25. The predicted waveform is similar to the flight test data, but there is an over prediction of 40%-60% in the peak-to-peak magnitude during the maneuver regime. This discrepancy is a result of over-prediction of the 5 and 6/rev torsional moment (Fig.26), which is driven by the over-prediction of dynamic stall peaks at the inboard blade locations. The predicted pitch-link load shows similar trend (Fig.27). The peak-to-peak magnitude of the structural loads predicted using the CFD/CSD and the lifting-line analyses is summarized in the Fig.28. In general CFD/CSD analysis is able to show better prediction for all the structural loads when compared with the lifting-line model. In particular, the peak-to-peak magnitude of the predicted pitch-link load is under-predicted by 50% during rev.14 using the lifting-line analysis, while the CFD/CSD analysis over-predicts it only by 15%. The over-prediction of peak pitch-link loads, during the revolutions 9-13 is due to premature stall onset in the CFD/CSD analysis.

Conclusions

A high load factor pull-up maneuver was analyzed using a Python-based simulation framework. The rotor control angles and the flight dynamic parameters (flight path and velocities, attitude angles and rates) were prescribed from flight test measurements (Counter 11029 of Black Hawk Airloads Program). A multibody finite element structural model was coupled in time to an unsteady RANS solver, and then to an unsteady lifting-line aerodynamic model to study the strengths and weaknesses of the traditional lifting-line analysis with the high-fidelity CFD/CSD simulation. The key conclusions from the present study are summarized here:

- The pull-up maneuver is characterized by the three distinct stall events as the rotor experiences load factors greater than 1.75g during the maneuver. The two dynamic stall events on the retreating side are predicted by the CFD/CSD analysis. The lifting- line analysis is unable to predict the high-frequency stall loads during the maneuver, especially the peak magnitude of pitching moment is under-predicted significantly.
- The advancing blade stall observed after revolution 12 onwards is not predicted by either of the analyses and depends on the accurate prediction of pitching moment from the previous revolution - not possible with current state-of-the-art.
- The predictions of the structural loads do not show the same level of correlation as the airloads when compared with flight test data. Even though the flap bending moment prediction looks satisfactory, the inability to predict the structural loads accurately is a problem even with steady flight analysis and is not an issue specific to the analysis of maneuvering flight.
- The CSD/lifting-line analysis is able to predict the general trends of the airloads time history during the maneuver, but is generally poor compared to the prediction capabilities of the coupled CFD/CSD simulation. However, the prediction of the dynamic stall events is better than the results found in the literature. The results clearly emphasize the need for a higher fidelity aerodynamic model in analysis of unsteady maneuvering flight.

References

1. Datta, A., Nixon, M. and Chopra, I., "Review of Rotor Loads Prediction with the Emergence of Rotorcraft CFD", Journal of the American Helicopter Society, Vol. 52, (4), October, 2007, pp. 287-217.

2. Kufeld, R. M., Balough, D. L., Cross, J. L., Studebaker, K. F., Jennison, C. D. and Bousman, W. G., "Flight Testing of the UH-60A Airloads Aircraft", American Helicopter Society, 50th Annual Forum Proceedings, Washington, D. C., May, 1994.

3. Bousman, W. G. and Kufeld, R. M., "UH-60A Airloads Catalogue",NASA/TM-2005-212827, AFDD/TR-05-003, August, 2005.

4. Bousman, W. G., "A Qualitative Examination of Dynamic Stall from Flight Test Data", Journal of the American Helicopter Society, Vol.43, (4), October, 1998, pp.279-295.

5. Kufeld, R. M., "High Load Conditions Measured on a UH-60A in Maneuvering Flight", Journal of the

American Helicopter Society, Vol. 43, (3), July, 1998, pp.202-211.

6. Washuta, K. W. and Stocker, B. P., "Air-to-Air Combat Test (AACT II) Maneuvering Flight Loads for UH-60A and AUH-76 Helicopters", USAAVSCOM TR-86-D-1, April, 1986.

7. Bhagwat, M. J., Ormiston, R. A., Saberi, H. A. and Xin, H., "Application of CFD/CSD Coupling for Analysis of Rotorcraft Airloads and Blade Loads in Maneuvering Flight", American Helicopter Society, 63rd Annual Forum Proceedings, Virginia Beach, VA, May, 2007.

8. Bhagwat, M. J. and Ormiston, R. A., "Examination of Rotor Aerodynamics in Steady and Maneuvering Flight Using CFD and Conventional Methods", American Helicopter Society Specialists' Conference on Aeromechanics, San Francisco, CA, January, 2008.

9. Abhishek, A., Datta, A. and Chopra, I., "Comprehensive Analysis, Prediction, and Validation of UH-60A Blade Loads in Unsteady Maneuvering Flight", American Helicopter Society, 63rd Annual Forum Proceedings, Virginia Beach, VA, May 1-3, 2007.

10. Abhishek, A., Datta, A. and Chopra, I., "Comprehensive Analysis, Prediction, andValidation of UH-60A Blade Loads in Unsteady Maneuvering Flight", AHS Helicopter Society Specialists' Conference on Aeromechanics, San Francisco, CA, January 23-25, 2008.

11. Yeo, H., "Investigation of Rotor Airloads and Structural Loads in Maneuvering Flight", American Helicopter Society, 64th Annual Forum Proceedings, Montreal, Canada, 29th April - 1st May, 2008.

12. Sitaraman, J. and Roget, B., "Prediction of Helicopter Maneuver Loads Using A Coupled CFD/CSD Analysis", The 26th Congress of International Council of the Aeronautical Sciences, September 14-19, 2008.

13. Thomas, S., Shreyas, A. and Baeder, J., "Wake coupling CFD-CSD Analysis of Helicopter Rotors in Steady and Maneuvering Flight Conditions", American Helicopter Society Aeromechanics Specialists' Conference, San Francisco, January, 2010.

14. Silbaugh, B. and Baeder, J. D., "Coupled CFD/CSD Analysis of a Maneuvering Rotor Using Staggered and Time-Accurate Coupling Schemes", American Helicopter Society Specialists' Conference on Aeromechanics, San Francisco, CA, January 23-25, 2008.

15. Abhishek, A., Datta, A. and Chopra, I., "Prediction of UH-60A Structural Loads Using Multibody Analysis and Swashplate Dynamics", Journal of Aircraft, Vol. 46, (2), March, 2009, pp.474-490.

16. Abhishek, A., "Modelling of Large Deformations in Rotors Using Second Order Beam Model Coupled to Multibody Formulation", 17th National Seminar on Aerospace Structures (NASAS), Indian Institute of Technology, Kanpur, September 22-24, 2011.

17. Hodges, D. H., "Geometrically Exact, Intrinsic Theory for Dynamics of Curved and Twisted Anisotropic Beams", AIAA Journal, Vol. 41, (6), June, 2003, pp.1131-1137; also "Erratum: Geometrically Exact, Intrinsic Theory for Dynamics of Curved and Twisted Anisotropic Beams", AIAA Journal, Vol.42, (7), July, 2004, p.1500.

18. Bauchau, O. A. and Kang, N. K., "A Multibody Formulation for Helicopter Structural Dynamic Analysis", Journal of the American Helicopter Society, Vol.38, (2), April, 1993, pp.3-14.

19. Reissner, E., "On One-Dimensional Large-Displacement Finite-Strain Beam Theory", Studies in Applied Mathematics, Vol.52, (2), April, 1973, pp.87-95.

20. Johnson, W., "Rotorcraft Dynamics Models for a Comprehensive Analysis", 54th Annual Forum, American Helicopter Society, Washington D.C., May 20-22, 1998.

21. Saberi, H., Khoshlahjeh, M., Ormiston, R.A. and Rutkowski, M. J., "Overview of RCAS and Application to Advanced Rotorcraft Problems", 4th Decennial Specialists' Conference on Aeromechanics, American Helicopter Society, San Francisco, CA, January, 2004.

22. Datta, A., "Fundamental Understanding, Prediction and Validation of Rotor Vibratory Loads in Steady-Level Flight", Ph.D. Dissertation, Department of

Aerospace Engineering, University of Maryland, College Park, MD, 2004.

23. Kufeld, R. M. and Johnson, W., "The Effects of Control System Stiffness Models on the Dynamic Stall Behavior of a Helicopter", Journal of the American Helicopter Society, Vol.45, (4), October, 2000, pp.263-269.

24. Weissinger, J., "The Lift Distribution of Swept-Back Wings", National Advisory Committee for Aeronautics, Technical Memorandum No.1120, 1947.

25. Leishman, J. G. and Beddoes, T. S., "A Semi-Empirical Model for Dynamic Stall", Journal of the American Helicopter Society, Vol.34, (3), July, 1989, pp.3-17.

26. Datta, A. and Chopra, I, "Validation of Structural and Aerodynamic Modeling Using UH-60A Airloads Program Data", Journal of the American Helicopter Society, Vol.51, (1), January, 2006, pp.43-58.

27. Ananthan, S. and Leishman, J. G., "Rotor Wake Aerodynamics in Large Amplitude Maneuvering Flight", Journal of the American Helicopter Society, Vol.51, (3), July, 2006, pp.225-244.

28. Yoon, S. and Jameson, A., "Lower-Upper Symmetric-Gauss-Seidel Method for Euler and Navier-Stokes Equations", AIAA Journal, Vol.26, (9), 1988, pp.1025-1026.

29. Pulliam, T., "Time Accuracy and the Use of Implicit Methods", AIAA-93-3360, 11th AIAA Computational Fluid Dynamics Conference, Orlando, FL, July, 1993.

30. Guruswamy, G. P. and Yang, T. Y., "Aeroelastic Time-Response Analysis of Thin Airfoils by Transonic Code LTRAN2", Computers and Fluids, Vol.9, (4), December, 1980, pp.409-425.

31. Datta, A. and Johnson, W., "An Assessment of the State-of-the-art in Multidisciplinary Aeromechanical Analyses", AHS Specialists' Conference on Aeromechanics, San Francisco, CA, January 23-25, 2008.

32. Tung, C., Caradonna, F. X. and Johnson, W., "Conservative Full Potential Model for Unsteady Transonic Rotor Flows", AIAA Journal, Vol.25, (2), 1987, pp.193-198.

33. Ananthan, S., Sitaraman, J., Baeder, J. D., Hahn, S., and Iaccarino, G., "Hybrid Unsteady Simulation of Helicopters: HUSH", 26th AIAA Applied Aerodynamics Conference, AIAA-2008-7339, Honolulu, HI, August 18-21, 2008.

34. Sitaraman, J., Datta, A., Baeder, J. D. and Chopra, I., "Fundamental Understanding and Prediction of Rotor Vibratory Loads in High-Speed Forward Flight", 29th European Rotorcraft Forum, September, 2003.

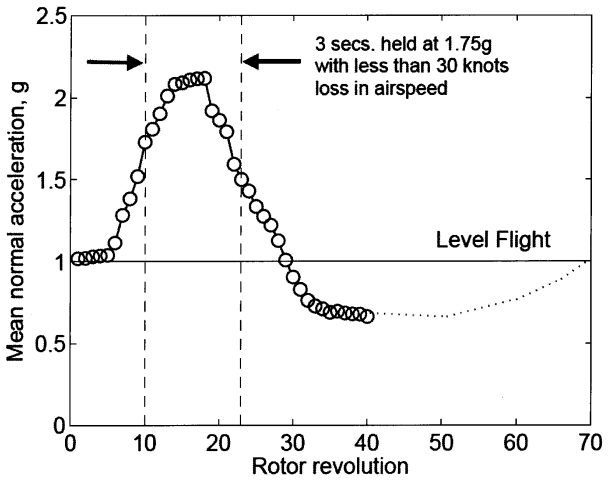

Fig.1 Measured Mean Load Factor

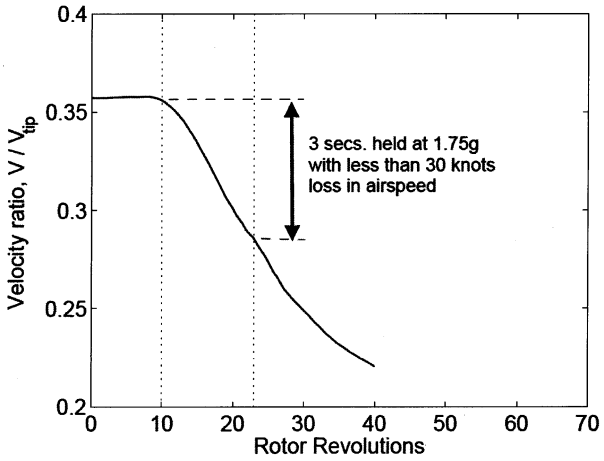

Fig.2 Measured Aircraft Velocity Ratio

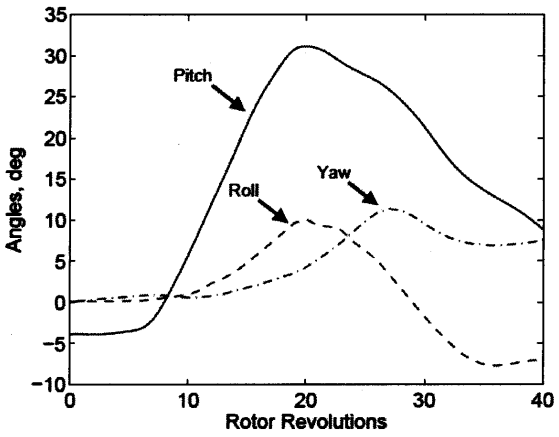

a) Attitude

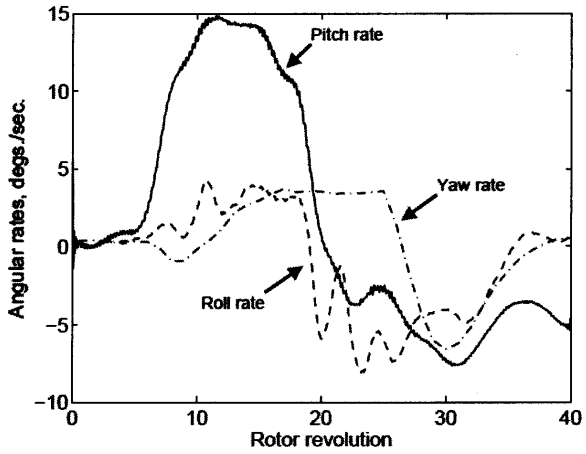

b) Rate

Fig.3 Measured Aircraft Attitude and Rates

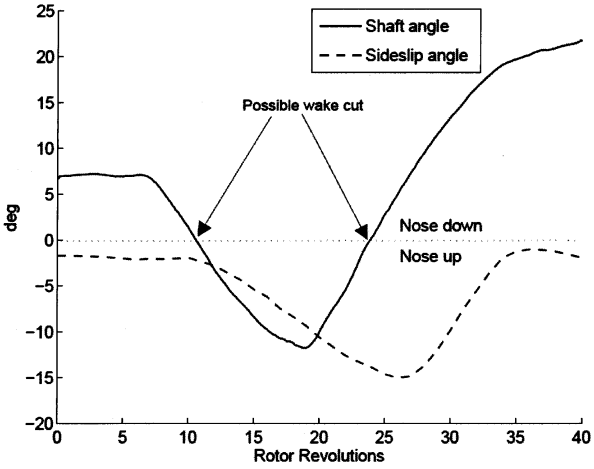

Fig.4 Aircraft Shaft Angle with respect to Oncoming Flow and Side-slip Angle

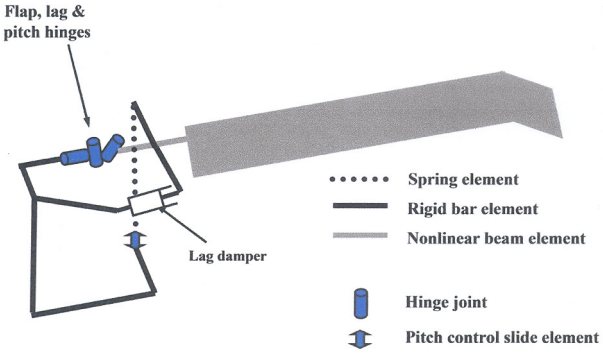

Fig.5 Schematic of the UH-60A Structural Model

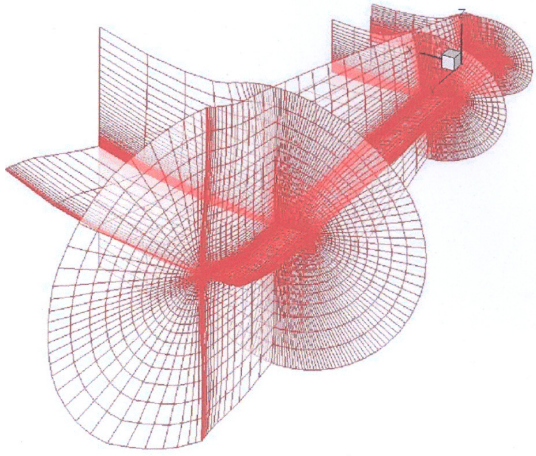

a) C-O body-fitted mesh

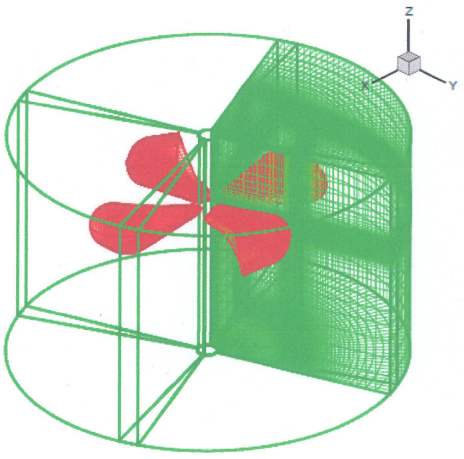

b) Computational domain with eight mesh system

Fig.6 Body Fitted Blade Meshes and the Cylindrical Off-body Meshes Used in the Overturns Solver

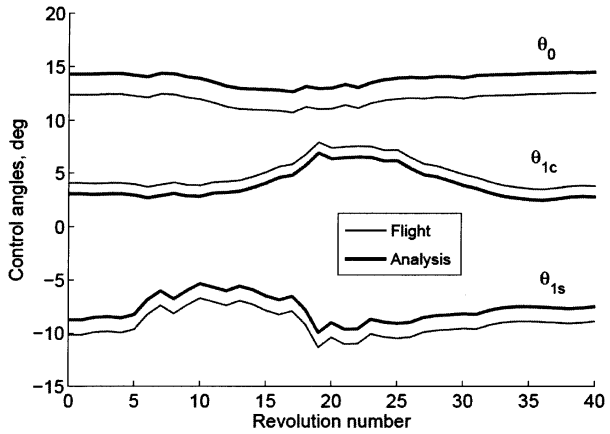

Fig.7 Prescribed Control Angles (Angles are adjusted to match the initial trim); Flight C11029

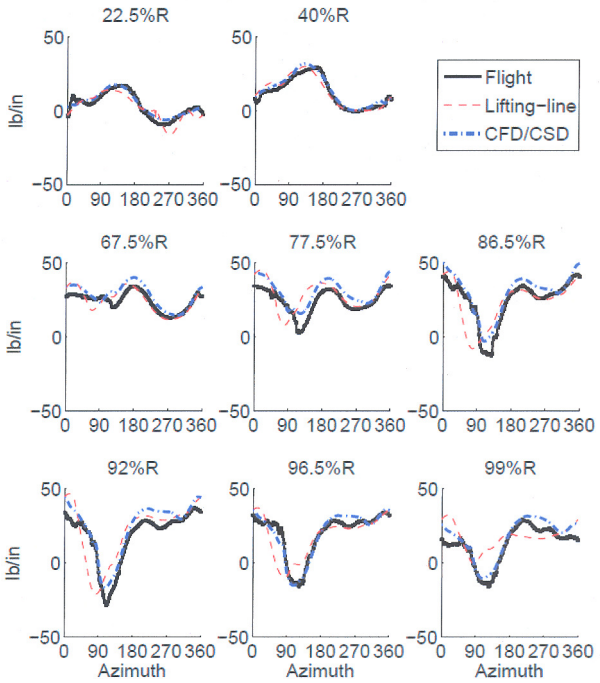

Fig.8 Predictions of the Normal Force for Steady Flight Regime (Rev 1) Predicted by Coupled Lifting-line Analysis and CFD/CSD

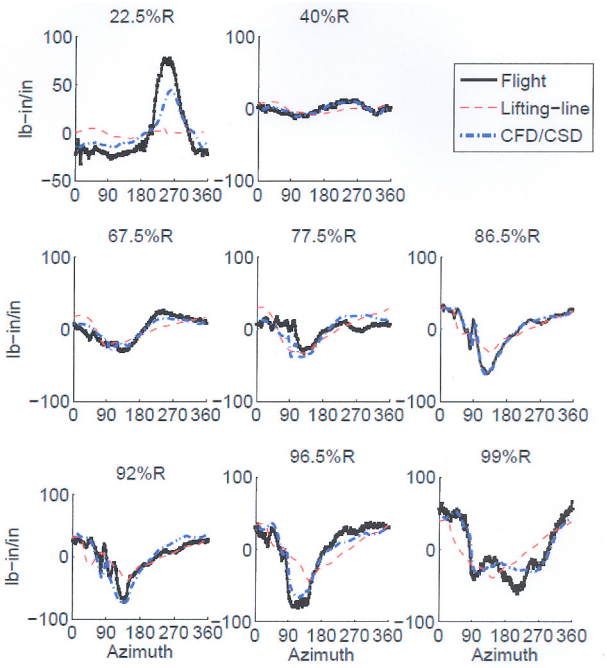

Fig.9 Predictions of the Pitching Moment (mean removed) for Steady Flight Regime (Rev 1) Predicted Using Coupled Lifting-line Analysis and CFD/CSD

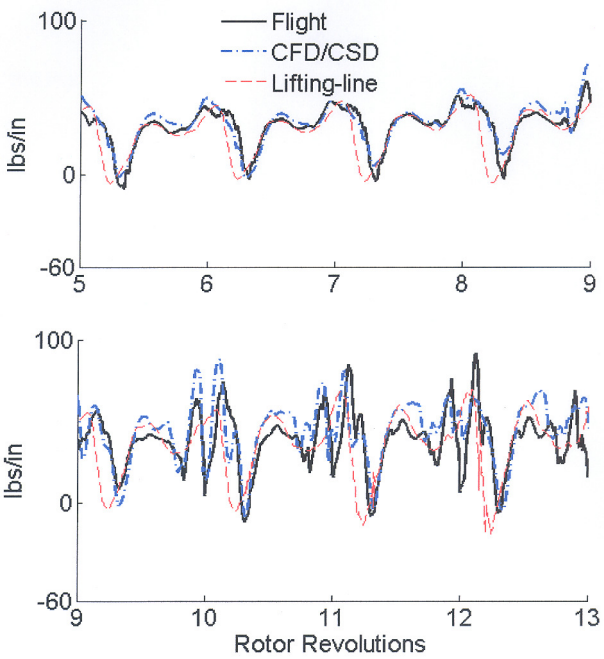

Fig.10 Predicted Normal Force Time History for the UTTAS Pull up Maneuver; Predictions Using Coupled Lifting-line and CFD/CSD at 86.5%R

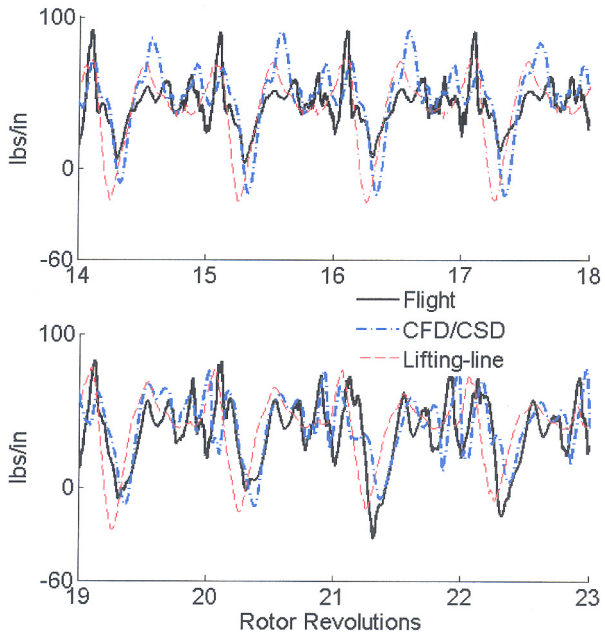

Fig.11 Predicted Normal Force Time History for the UTTAS Pull up Maneuver ; Predictions Using Coupled Lifting-line and CFD/CSD at 86.5%R

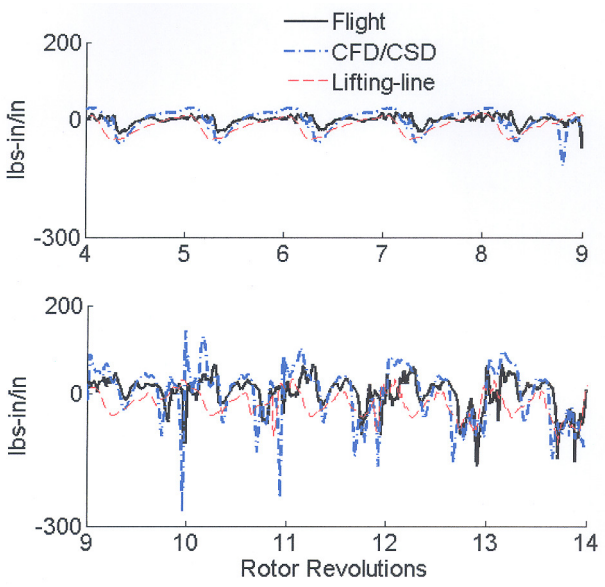

Fig.12 Predicted Pitching Moment (mean removed) for the UTTAS Pull up Maneuver; Predictions Using Coupled Lifting-line Analysis and CFD/CSD at 77.5%R

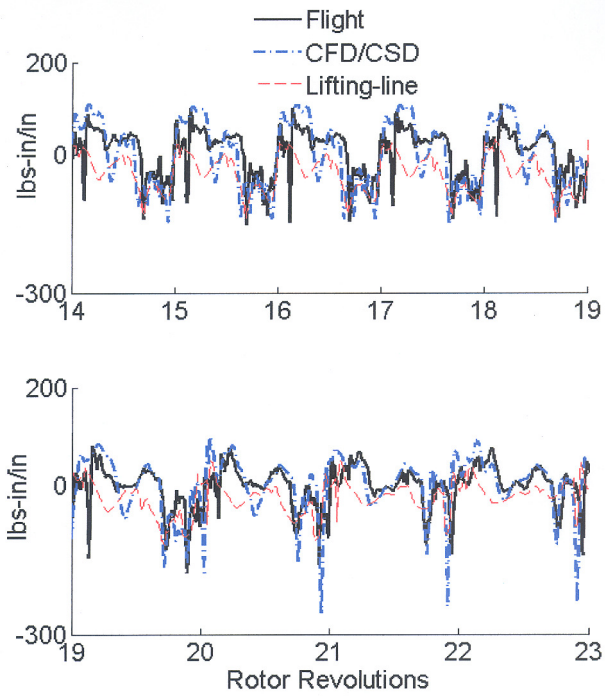

Fig.13 Predicted Pitching Moment (mean removed) for the UTTAS Pull up Maneuver; Predictions Using Coupled Lifting-line Analysis and CFD/CSD at 77.5%R

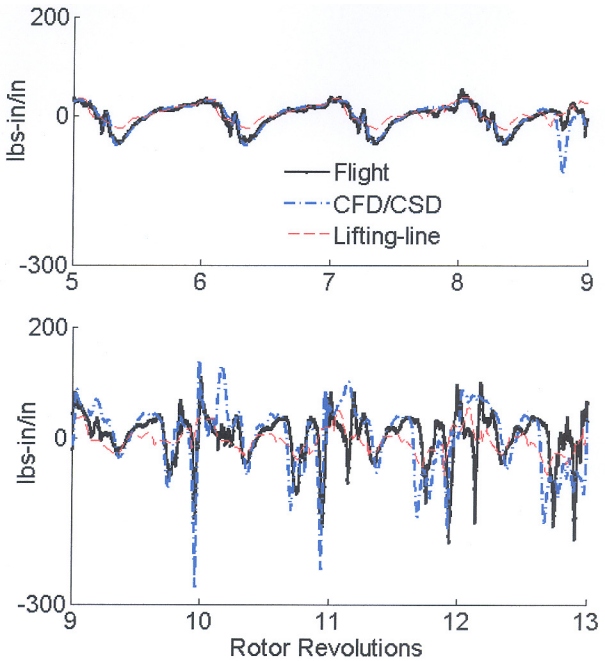

Fig.14 Predicted Pitching Moment (mean removed) for the UTTAS Pull up Maneuver; Predictions Using Coupled Lifting-line Analysis and CFD/CSD at 86.5%R

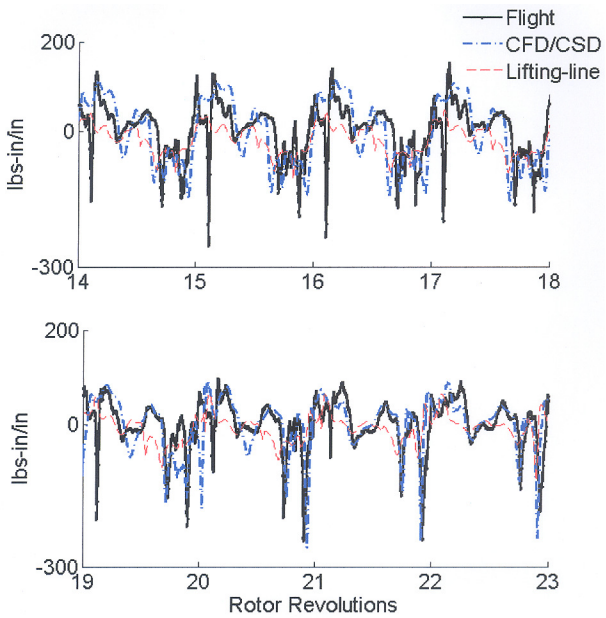

Fig.15 Predicted Pitching Moment (mean removed) for the UTTAS Pull up Maneuver; Predictions Using Coupled Lifting-line Analysis and CFD/CSD at 86.5%R

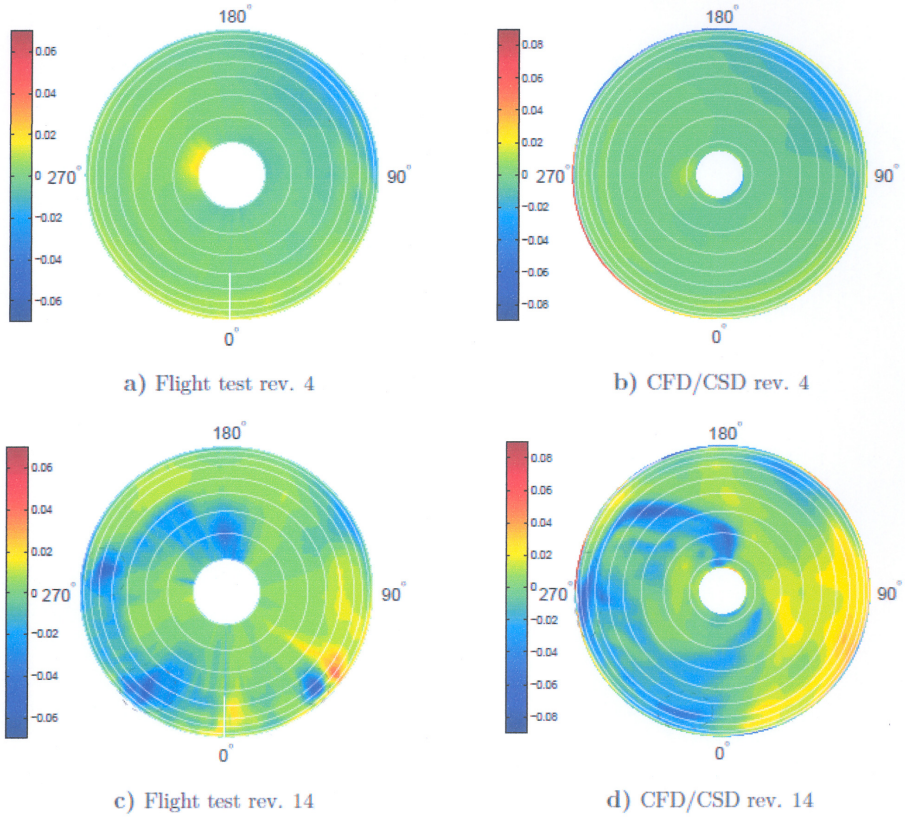

Fig.16 Contour Plots of the Non-dimensional Aerodynamic Pitching Moments (mean removed) During Revs.4 and 14 of the UTTAS Pull-up Maneuver Predicted by CSD Coupled with CFD

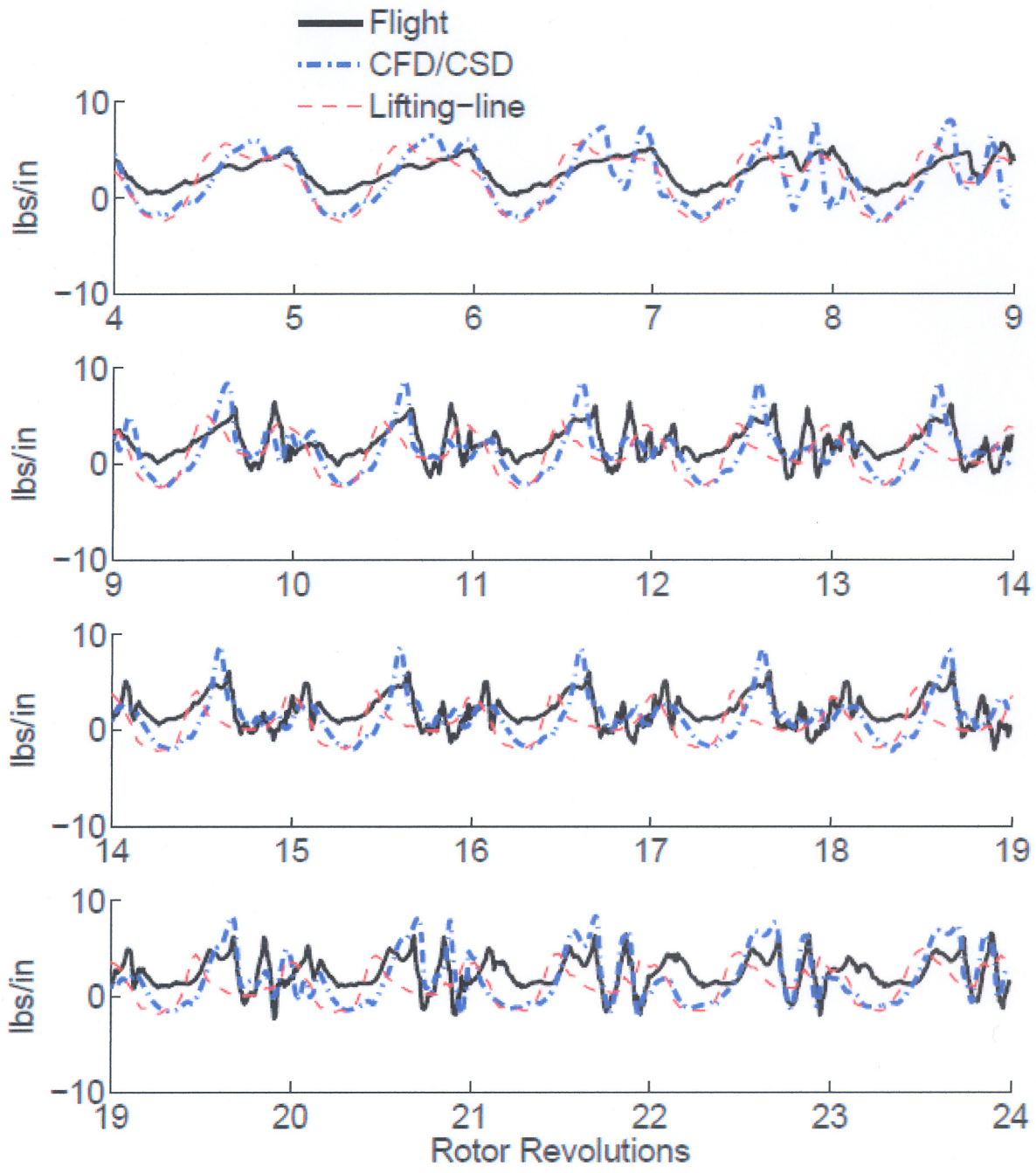

Fig.17 Predicted Chord Force Time History for the UTTAS Pull up Maneuver; Predictions Using Lifting-line Analysis and CFD/CSD at 86.5%R

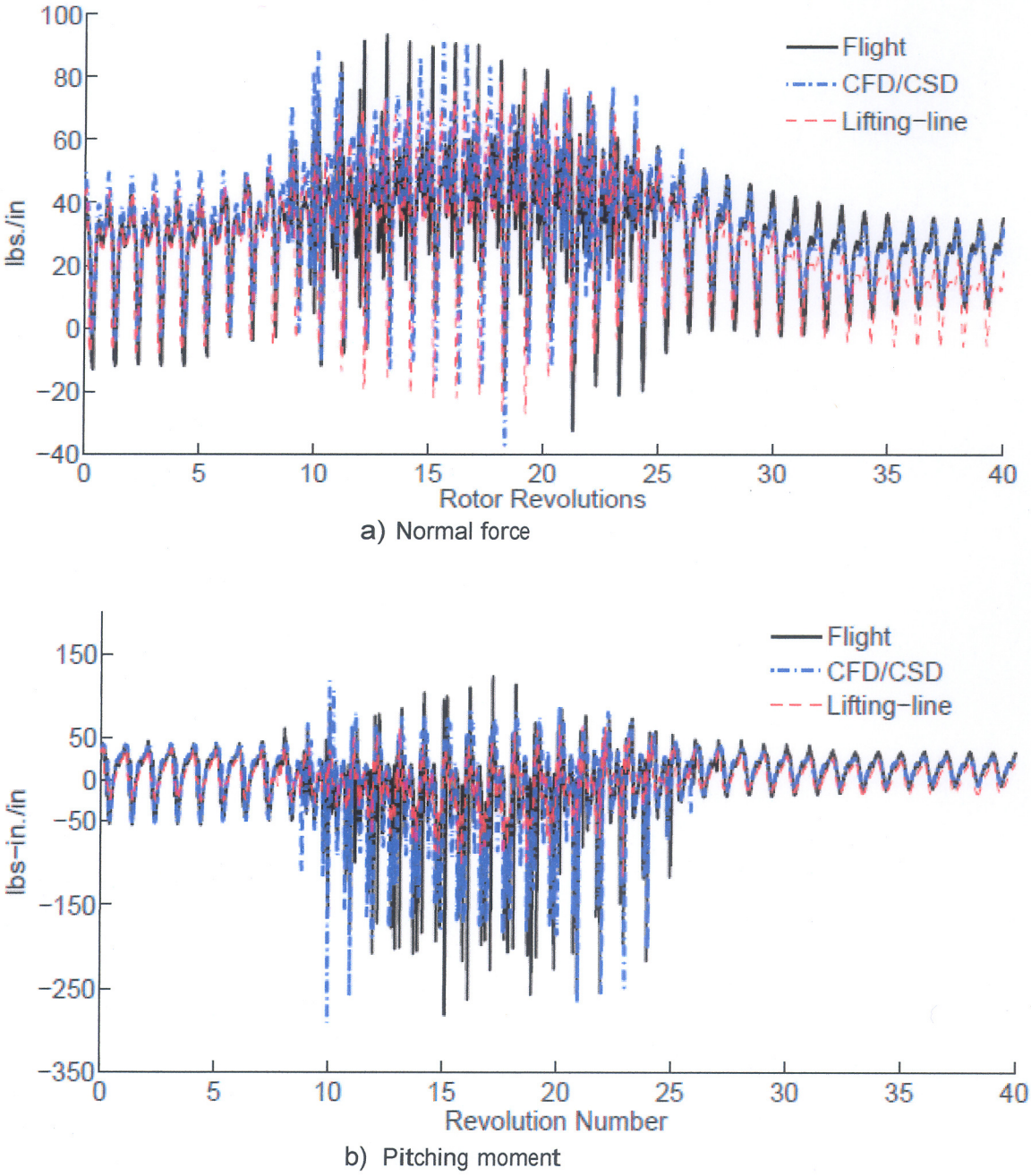

Fig.18 Comparison of the CFD/CSD and Coupled Lifting-line Simulations Showing the Lift Deficiency in Prediction at 86.5%R

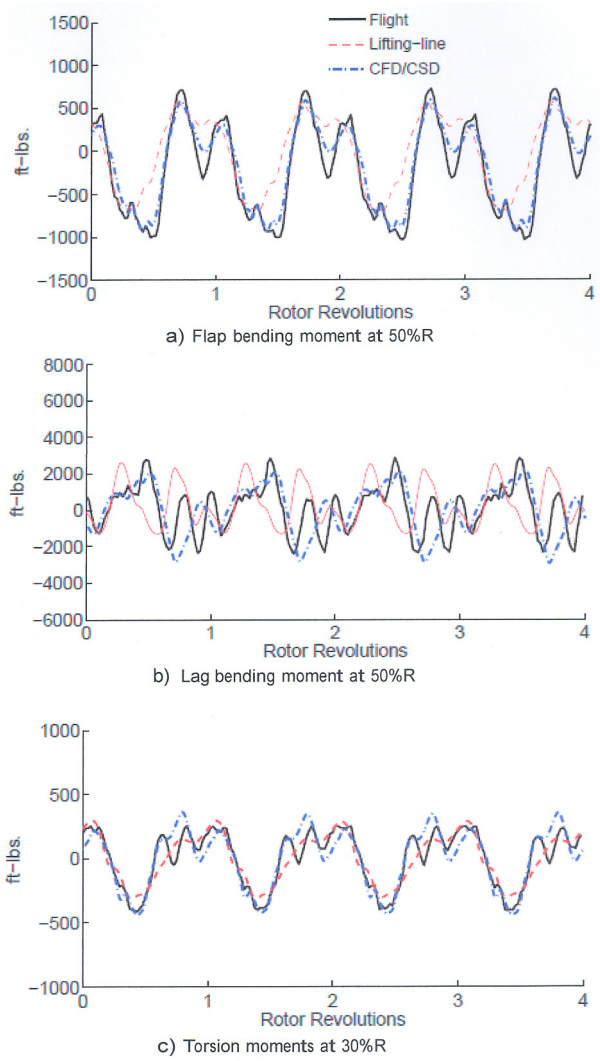

Fig.19 Predicted Flap, Lag and Torsional Moment Time Histories (mean removed), for the Steady Flight Regime Using Coupled Lifting-line and CFD/CSD

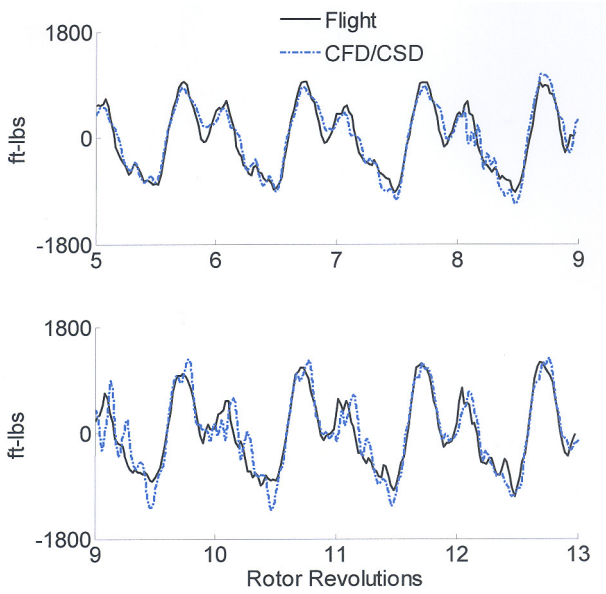

Fig.20 Predicted Sectional Flap Bending Moment (mean removed) Time Histories for the UTTAS Pull up Maneuver Using CFD/CSD at 50%R

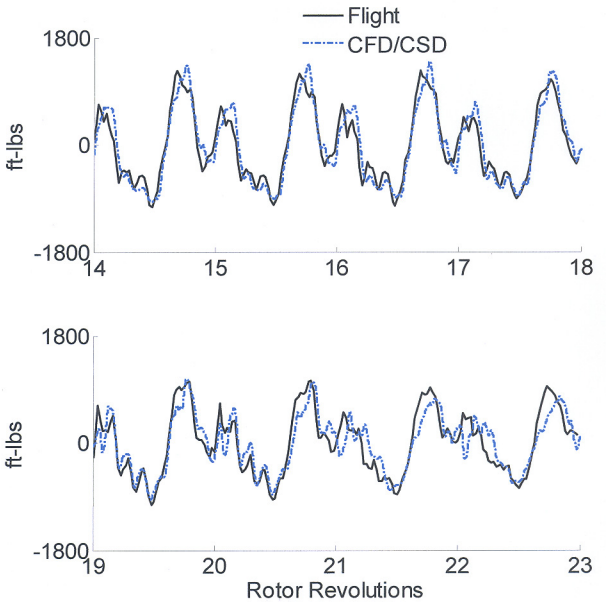

Fig.21 Predicted Sectional Flap Bending Moment (mean removed) Time Histories for the UTTAS Pull up Maneuver Using CFD/CSD at 50%R

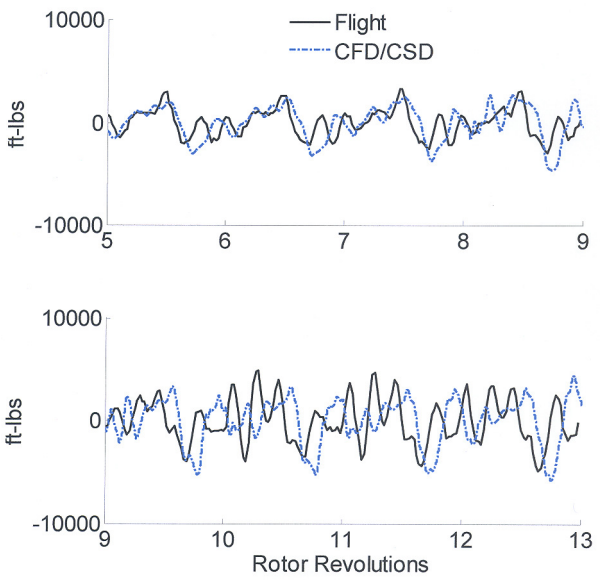

Fig.22 Predicted Sectional Lag Bending Moment (mean removed) Time Histories for the UTTAS Pull up Maneuver Using CFD/CSD at 50%R

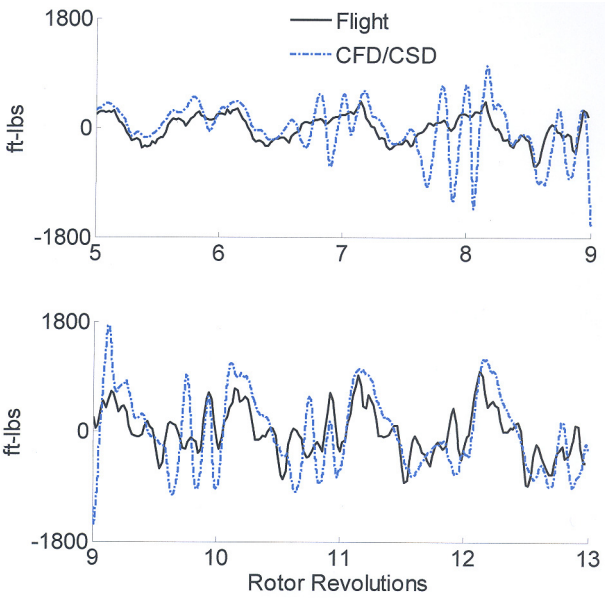

Fig.24 Predicted Sectional Torsional Moment (mean removed) Time Histories for the UTTAS Pull up Maneuver Using CFD/CSD at 30%R

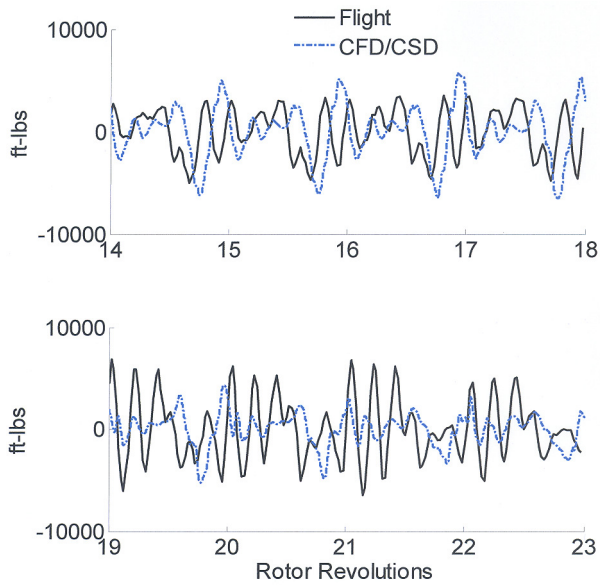

Fig.23 Predicted Sectional Lag Bending Moment (mean removed) Time Histories for the UTTAS Pull up Maneuver Using CFD/CSD at 50%R

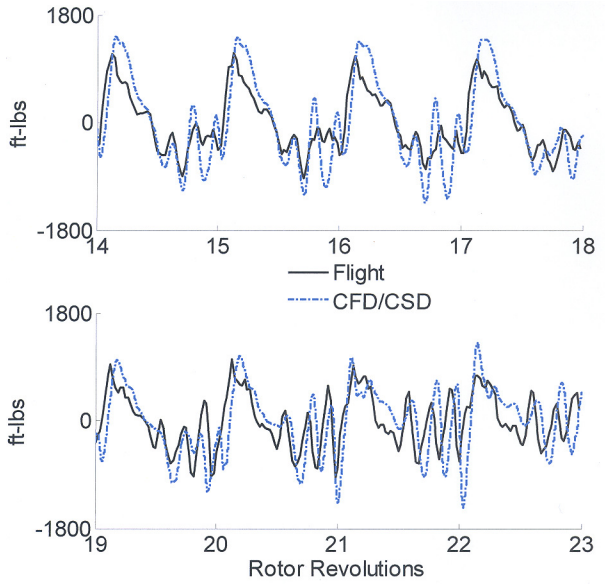

Fig.25 Predicted Sectional Torsional Moment (mean removed) Time Histories for the UTTAS Pull up Maneuver Using CFD/CSD at 30%R

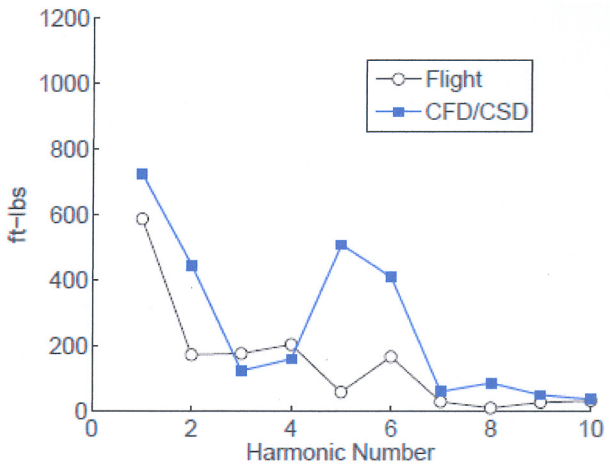

Fig.26 Torsional Moment Harmonics at 30%R for the Rev.14; Prediction Using CFD/CSD

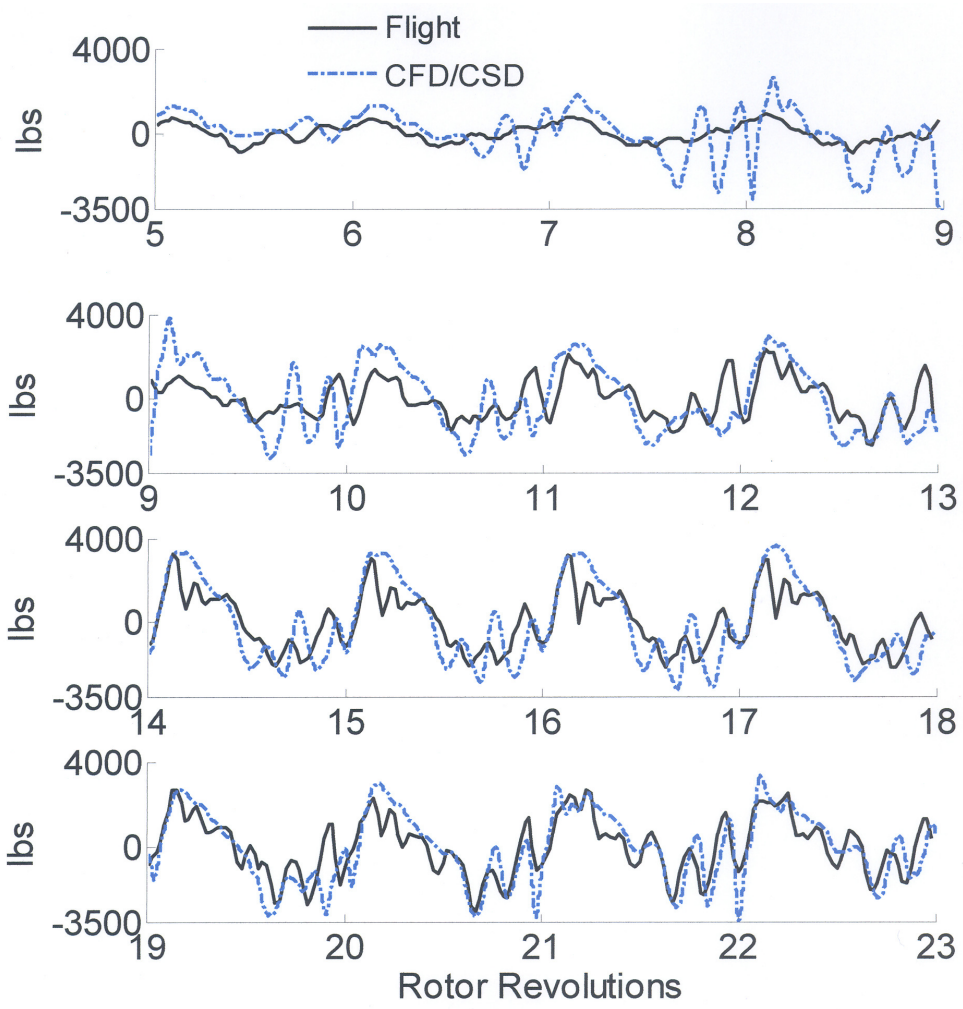

Fig.27 Predicted Pitch-link Load (mean removed) Time Histories for the UTTAS Pull up Maneuver Using CFD/CSD

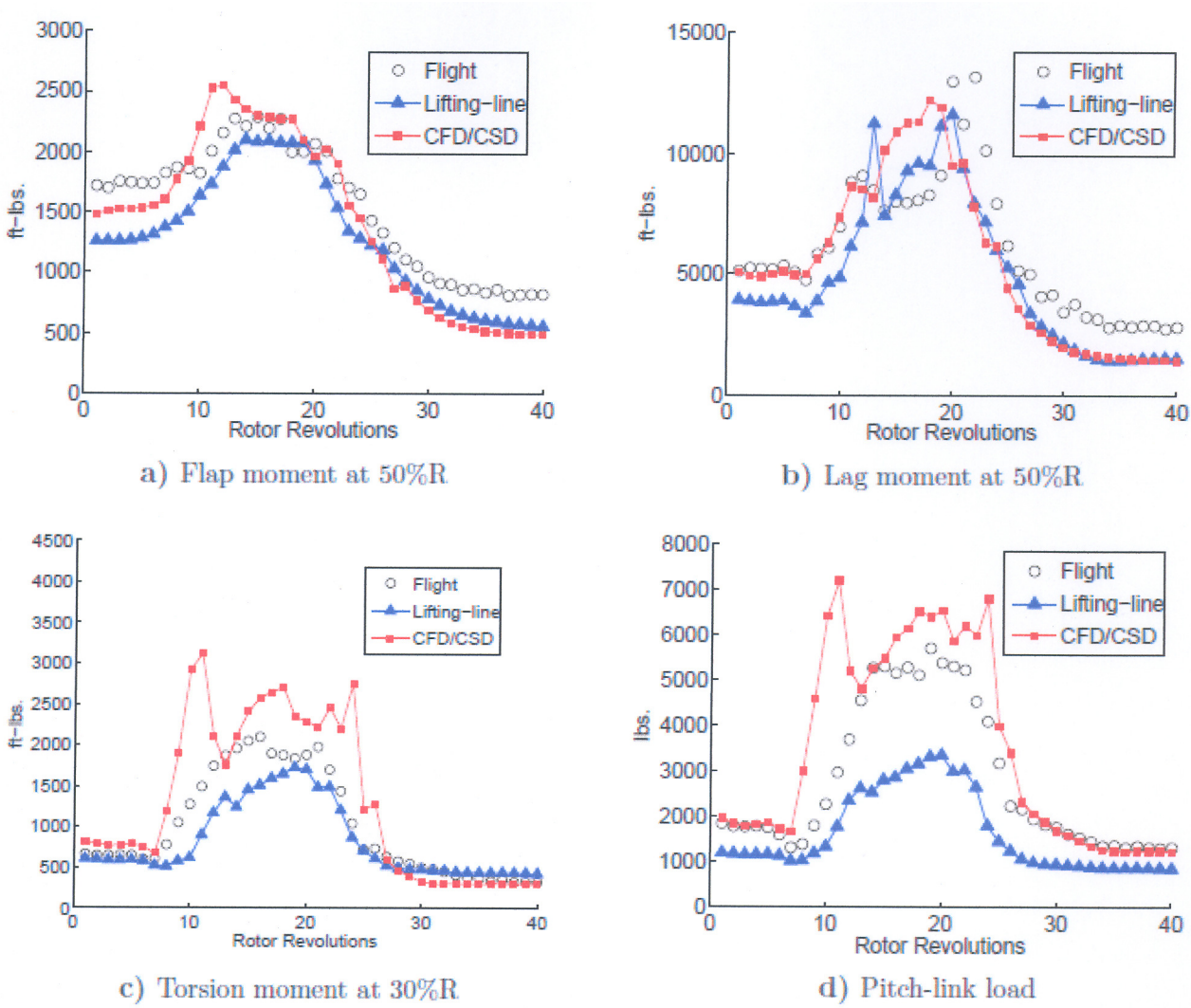

Fig.28 Summary of Structural Loads Predicted Using Coupled Lifting-line Analysis and CFD/CSD